Supporting information for

Gene-driven Self-morphing Microtubule-based Active Matter

Rochelle Silverman[1], Erez Zerbib[1], Hillel Aharoni[2], Vincent Noireaux[3], Alexandra M. Tayar[1*]

[1]Chemical and Biological Physics Department, Weizmann Institute of Science, Rehovot 7610001, Israel

[2]Department of Complex systems, Weizmann Institute of Science, Rehovot 7610001, Israel

[3]School of Physics and Astronomy, University of Minnesota, 115 Union Street SE, Minneapolis, Minnesota 55455, United States

[*]e-mail: alexandra.tayar@weizmann.ac.il

This PDF file includes:

Materials and Methods

1. Microtubule purification and assembly

1.1 **Tubulin extraction and purification:** Tubulin was purified from porcine brain tissue (Lahav Research Institute) using two cycles of temperature-dependent polymerization and depolymerization, following an adapted high-molarity buffer protocol[1–4]. Fresh brains were transported on ice in PBS (20 mM sodium phosphate, pH 7.2, 150 mM NaCl). After removal of meninges and blood clots, the tissue was homogenized in ice-cold depolymerization buffer (DB; 50 mM MES, pH 6.6, 1 mM $CaCl_2$) at a ratio of 1 L/kg. The homogenate was clarified by centrifugation at 10,000 × g for 60 min at 4 °C.

1.2 **Tubulin Recycling:** The supernatant was mixed with an equal volume of pre-warmed (37 °C) high-molarity PIPES buffer (HMPB; 1 M PIPES, pH 6.9, 10 mM $MgCl_2$, 20 mM EGTA) and supplemented with ATP (1.5 mM final) and GTP (0.5 mM final). Glycerol was added to a final concentration of 33% (v/v) to promote polymerization. The mixture was incubated at 37 °C for 1 h, and polymerized microtubules (MTs) were collected by ultracentrifugation at 151,000 × g for 30 min at 37 °C.

The resulting pellet was resuspended in ice-cold depolymerization buffer and incubated on ice for 30 min to induce depolymerization, followed by clarification at 70,000 × g for 30 min at 4 °C. A second polymerization cycle was then performed by repeating the addition of HMPB, nucleotides, and glycerol under the same conditions.

1.3 **Final buffer exchange and storage of tubulin**: The final MT pellet was collected at 151,000 × g and resuspended in ice-cold BRB80 buffer (80 mM PIPES, pH 6.8, 1 mM $MgCl_2$, 1 mM EGTA). After a final clarification at 104,000 × g (4 °C), the tubulin concentration was determined spectrophotometrically (ε_{280} = 115,000 $M^{-1}cm^{-1}$). Aliquots were flash-frozen in liquid nitrogen and stored at -80°C.

1.4 **Tubulin labeling:** Tubulin was labeled with Alexa Fluor 647 (Thermo Fisher, A20006) using a polymerization-depolymerization method adapted from a previously published protocol[2]. Tubulin (10 mg/mL) was first polymerized at 37 °C for 30 min in the presence of 3 mM GTP and 0.5 mM DTT. Polymerized MTs were pelleted through a high-pH cushion buffer (100 mM HEPES, pH 8.6, 1 mM $MgCl_2$, 1 mM EGTA, 60% glycerol (v/v)) by ultracentrifugation at 300,000 × g for 30 min at 37 °C.

The resulting pellet was resuspended in labeling buffer (100 mM HEPES, pH 8.6, 1 mM $MgCl_2$, 1 mM EGTA, 40% glycerol (v/v)) and incubated with a 15-fold molar excess of AF647 for 30 min at 37 °C. The reaction was quenched by addition of an equal volume of quench buffer (2× BRB80, 100 mM K-glutamate, 40% glycerol (v/v)).

Labeled microtubules were recovered by a second ultracentrifugation through a low-pH cushion buffer (BRB80, 60% glycerol (v/v)) at 300,000 × g for 30 min at 37 °C. The pellet was rinsed with

warm M2B buffer (80 mM PIPES, pH 6.8, 2 mM $MgCl_2$, 1 mM EGTA) and subsequently depolymerized on ice for 30 min. The solution was clarified by ultracentrifugation at 300,000 × g for 10 min at 4 °C.

Tubulin concentration and labeling efficiency were determined spectrophotometrically (ε_{280} = 115,000 $M^{-1}cm^{-1}$ for tubulin; ε_{647} = 270,000 $M^{-1}cm^{-1}$ for AF647). Labeled tubulin was aliquoted, flash-frozen in liquid nitrogen, and stored at -80 °C.

1.5 **Microtubule polymerization:** Fluorescently labeled MTs were polymerized from a mixture of unlabeled and Alexa Fluor 647-conjugated tubulin, with labeled tubulin comprising 2% molar ratio of the total tubulin concentration. The tubulin mixture was prepared at a final concentration of 8 mg/mL in M2B buffer (80 mM PIPES, pH 6.8, 2 mM $MgCl_2$, 1 mM EGTA), supplemented with 20 mM DTT and 10 mM guanosine-5′-(α,β-methyleno)triphosphate (GMPCPP). GMPCPP, a non-hydrolysable GTP analogue, was used to promote the formation of stable MTs. Polymerization was initiated by incubation at 37 °C for 30 min, followed by an additional 5 h incubation at room temperature to allow the microtubules to reach a steady-state length distribution. The resulting MTs were aliquoted, flash-frozen in liquid nitrogen, and stored at -80 °C until use.

2. **GamS purification:** To enhance protein yields in the cell-free expression system, the GamS protein from bacteriophage λ was expressed and purified[2,5]. His-tagged GamS (~13 kDa) was expressed in *E. coli* BL21 (DE3) from a pBAD plasmid. Cells were grown in LB medium supplemented with 100 µg/mL ampicillin at 37 °C and induced at an OD_{600} of 0.4–0.6 with 0.25% L-arabinose for 2 h. Cells were harvested by centrifugation at 8,000 × g. Cell pellets were resuspended in binding buffer (50 mM sodium phosphate, pH 8.0, 300 mM NaCl, 10 mM imidazole) and lysed by sonication. The lysate was clarified by centrifugation at 33,000 × g for 60 min at 4 °C. The supernatant was loaded onto a 5 mL HisTrap affinity column (17-5248-02, Cytiva, Uppsala, Sweden) and washed with binding buffer. GamS was eluted using a linear imidazole gradient up to 500 mM. The purified protein was concentrated using a 3 kDa MWCO centrifugal filter (Millipore) and buffer-exchanged into 10 mM Tris-HCl (pH 7.5). Protein concentration was determined spectrophotometrically (ε_{280} = 11,460 $M^{-1}cm^{-1}$). Aliquots were flash-frozen in liquid nitrogen and stored at -80 °C.

3. **deGFP purification:** His-tagged deGFP (~27 kDa) was expressed in *E. coli* Rosetta cells. Cultures were grown in LB medium supplemented with 100 µg/mL ampicillin and 50 µg/mL chloramphenicol at 37 °C to an OD_{600} of 0.6-0.8, then induced with 1 mM IPTG and incubated overnight at 18 °C. Cells were harvested by centrifugation at 8,000 × g for 20 min at 4 °C and resuspended in binding buffer (50 mM sodium phosphate, pH 8.0, 300 mM NaCl, 10 mM imidazole). Cells were lysed by sonication, and the lysate was clarified by centrifugation at 33,000 × g for 30 min at 4 °C. The supernatant was loaded onto a Ni-NTA affinity column (17-5248-02, Cytiva, Uppsala, Sweden), washed with binding buffer, and eluted using a linear imidazole gradient up to 500 mM. For further purification, the protein was subjected to size-exclusion

chromatography (SEC) on a Superdex 75 column (Cytiva, Uppsala, Sweden) equilibrated in PBS (50 mM sodium phosphate, pH 7.4, 150 mM NaCl). Peak fractions were pooled and concentrated using a 10 kDa MWCO centrifugal filter (Millipore). Protein concentration was determined spectrophotometrically (ε_{280} = 55,000 $M^{-1}cm^{-1}$). Aliquots were flash-frozen in liquid nitrogen and stored at -80 °C.

4. **T7 RNA polymerase purification:** His-tagged T7 RNA polymerase (~100 kDa) was expressed in *E. coli* BL21 (DE3) from the pBH161 plasmid[6]. Cells were grown in 1 L of LB medium supplemented with 100 µg/mL ampicillin at 37 °C to an OD_{600} of ~0.5, induced with 1 mM IPTG, and incubated overnight at 4 °C. Cells were harvested by centrifugation at 8,000 × g for 30 min at 4 °C and resuspended in binding buffer (50 mM sodium phosphate, pH 8.0, 300 mM NaCl, 10 mM imidazole). Cells were lysed by sonication, and the lysate was clarified by centrifugation at 33,000 × g for 40 min at 4 °C. The supernatant was loaded onto a 5 mL HisTrap affinity column (17-5248-02, Cytiva, Uppsala, Sweden), washed with binding buffer, and the protein was eluted using a linear imidazole gradient up to 500 mM. For further purification, size-exclusion chromatography (SEC) was performed on a Superdex 200 column (Cytiva, Uppsala, Sweden) equilibrated in storage buffer (50 mM Tris-HCl, pH 7.5, 100 mM NaCl, 1 mM DTT). Peak fractions were pooled and concentrated using a 50 kDa MWCO centrifugal filter (Millipore). Protein concentration was determined spectrophotometrically (ε_{280} = 160,660 $M^{-1}cm^{-1}$). Aliquots were flash-frozen in liquid nitrogen and stored at -80 °C.

5. ***E. coli* lysate-based cell-free transcription-translation system:** The cell-free gene expression (CFE) reactions used in this work were based on the CFE toolbox 2.0[5]. The lysate was prepared from the *E. coli* strain BL21-ΔrecBCD Rosetta2, which has a recBCD knockout to prevent the degradation of linear DNA[7]. Briefly, cells were grown in 2xYT medium supplemented with phosphates, pelleted, washed, and lysed using a cell press. The lysate was centrifuged, and the supernatant was incubated at 37 °C for 80 min. After a second centrifugation, the supernatant was dialyzed at 4 °C for 3 h. The dialyzed lysate was centrifuged, aliquoted, and stored at -80 °C. The volume of the CFE reactions consisted of 33% cell lysate, and 67% of the other components (energy mix, and amino acids). The reaction buffer included 50 mM Hepes (pH 8), 1.5 mM ATP and GTP, 0.9 mM CTP and UTP, 0.26 mM coenzyme A, 0.33 mM NAD, 0.75 mM cAMP, 0.068 mM folinic acid, 1 mM spermidine, 30 mM 3-phosphoglyceric acid (3-PGA), 1 mM dithiothreitol (DTT), 1.5% PEG8000, and 20-40 mM maltodextrin. Amino acids were added at concentrations between 1.5 mM and 6 mM for each of the 20 amino acids. Magnesium (4 mM) and potassium (75 mM) concentrations were set for maximum deGFP synthesis.

6. **MT-CFE mixture:** Gene expression was performed using the E. coli lysate-based cell-free transcription-translation system. A master extract mix was prepared by supplementing pre-packed ToolBox 2 *E. coli* extract with 3.5 mM of ATP, 0.8 mM IPTG, 7 µM purified GamS, 1.5 mM $MgCl_2$, 0.1 µM purified T_7RNA polymerase, 0.7% PEG 35 kDa (w/v) and 0.5 mg/mL fluorescently labeled MTs. The master mix was aliquoted into individual reactions and supplemented with DNA, provided either as plasmids or linear PCR products, encoding the desired genes at final

concentrations ranging from 0.5 to 100 nM depending on the experimental condition. Each reaction had a total volume of 12 µL, consisting of 10 µL of lysate mix and the remaining volume made up of DNA diluted in DDW. Reactions were assembled in wells with a ~100 µL air layer above the solution.

7. **Multi-well plate compartment for microscopy imaging:** Prepared reaction mixtures were transferred into a Greiner Bio-One Cell-Repellent 384-well black plate with a µClear bottom. Wells were sealed with an OptiSeal optical adhesive film and centrifuged at 100 × g for 5 min at room temperature to remove air bubbles and promote MT sedimentation prior to fluorescence imaging.

8. **Imaging:** Fluorescence imaging was performed on an inverted Nikon Ti2 microscope equipped with an ORCA-Fusion CMOS camera (C14440-20UP/C15440-20UP). Images were acquired using either a 20× APO Fluor objective (NA 0.8), a 10× Plan APO objective (NA 0.45), or a 4× Plan Apo objective (NA 0.45).

9. **3D printing:** Wells with protrusions were fabricated using a microArch S240A 3D printer (Boston Micro Fabrication) and BIO Resin Y-10 (Boston Micro Fabrication) (MS Fig. 4). Printing was performed with a layer height of 10 µm using the manufacturer's recommended settings. After printing, parts were washed with ethanol in a Form Wash (Formlabs) for 10-20 min prior to removal from the build plate. The parts were then separated from the build plate rinsed by submersion and sonication in clean ethanol (three cycles of 3 min each at 30 °C). The parts were rinsed with fresh ethanol and then dried thoroughly using compressed nitrogen gas. They were post-cured for 5 min on each side using a CureZone MKI II Light Cure Box (Creative Cadworks, 65 W). To produce an optically clear base, a drop of uncured resin was placed on a clean, scratch-free glass slide. The printed structure was positioned base-down onto the resin and gently pressed to eliminate air bubbles. Magnets were used to maintain uniform contact between the structure and the glass. The assembly was then cured in a RC-2 Resin Curing Enclosure (Sunlu, 42 W) for 10 min with the structure facing upward. The structure was subsequently removed from the glass and post-cured upside down in the CureZone MKI II Light Cure Box (Creative Cadworks, 65 W) for an additional 5 min.

3D printed device passivation: To ensure compatibility with biological samples, printed parts were passivated by soaking in a 1.3% (w/v) BSA in PBS for 30 min at room temperature. After incubation, parts were rinsed twice with Milli-Q water, dried with compressed nitrogen gas, and further dried using an 8 min drying cycle in a RC-2 Resin Curing Enclosure (Sunlu).

3D printed device recycling: After use, printed parts were cleaned by stirring in 1% (v/v) Hellmanx III (Hellma Analytics) for 30 min. The parts were then rinsed twice with Milli-Q water, dried with compressed nitrogen gas, and stored for reuse.

10. **Plasmids and DNA preparation:** All constructs used in this study are listed in **Table S1**. Constructs were either obtained from Addgene or generated in-house using standard molecular

cloning techniques. Reporter and regulatory elements were based on established *E. coli* transcriptional systems, including T7 and σ^{70} (p_{70}) promoters, while motor constructs were derived from the chimeric kinesin KIF3A (Addgene plasmid # 129768).

Several constructs were engineered specifically for this study. The pT7-deGFP plasmid was generated by replacing the σ^{70} promoter of Addgene #40019 with a T7 promoter via QuikChange mutagenesis. Fusion constructs, including kinesin-deGFP and kinesin-σ^{28}, were assembled using Gibson cloning from existing templates. To ensure consistent behavior of fusion proteins, all kinesin-transcription factor and kinesin-reporter constructs were designed with a flexible linker (GTGSGS). Additional variants were generated by promoter exchange or by introducing degradation tags (SsrA) at the C-terminus via PCR. Together, this library of constructs enables independent and combinatorial control of motor activity, gene expression, and regulatory feedback within the cell-free system.

The p_{70}-PRC1 construct was generated by PCR amplification of the PRC1 coding sequence using KAPA HiFi polymerase (KAPA Biosystems). A forward primer containing the σ^{70} (p_{70}) promoter sequence was designed (IDT), enabling promoter insertion during amplification. The PRC1 sequence was amplified from plasmid gifted from Subramanian Lab [8], and the resulting product was used for downstream cloning.

2. Data Analysis

2.1 **Particle image velocimetry (PIV)**: Mean velocity magnitudes were calculated from velocity fields obtained via PIV analysis of MT fluorescence image sequences using PIVlab 3.01 (MATLAB R2023b). PIV analysis parameters, including interrogation window size and number of passes, were selected using the program-recommended settings based on the segment of each video exhibiting the fastest flows to ensure adequate capture of the full velocity range. For each time step, velocity fields were computed from consecutive image frames. The focal plane was set at the top of the initial MT sheet to minimize any effects of surface adhesion to the well bottom. Velocity vectors from low-contrast regions were excluded from mean velocity magnitude calculations.

2.2 **Wavelength analysis:** The focal plane for instability wavelength analysis was determined from the intensity profile of the undeformed MT sheet. At the first acquisition time point, the mean pixel intensity was calculated for each z-slice and plotted as a function of z-index. The z-plane at or near the peak intensity was selected for all subsequent analyses performed in MATLAB. This methodology was used for the data in MS Figs. 1 and 4.

> **Image preprocessing and blister bending detection:** Raw grayscale x-y images were converted to double precision and inverted so that dark regions appeared bright. Noise was reduced using 5 iterations of anisotropic diffusion filtering to preserve edges while smoothing homogeneous regions. Edges were detected using a Sobel operator with an adaptive threshold scaled by a user-defined factor (fudgeFactor), adjusted for imaging

conditions (objective, modality, and exposure) in MATLAB. The binary edge map was refined by sequential dilation (linear and disk structuring elements), followed by hole filling and morphological closing to improve boundary continuity and remove small artifacts. Objects below a minimum area threshold (set by magnification) and those touching image borders were excluded. Connected components were then labeled, and region properties (centroid, area, orientation, perimeter, and pixel indices) were extracted using the built-in function regionprops.

Definitions of blister geometry:

Area: The area of each blister was defined as the number of pixels within each filled binary region.

Length: Blister masks were skeletonized (bwskel, MATLAB), and the longest geodesic path was identified and extended to the object boundary. Length was calculated as the cumulative Euclidean distance along this path.

Width: Blister width was computed as the mean perpendicular distance between boundaries along a smoothed (Savitzky-Golay, MATLAB) skeleton. Measurements were taken at up to 20 points along the original skeleton; if fewer valid points were available, the perpendicular distances at all valid points were averaged.

Tracking across frames: Each blister was tracked over time using its centroid position, geometric properties (width, length, orientation), object mask, and a Kalman filter for motion prediction. A constant-velocity Kalman filter was initialized upon first detection of each blister. Objects associations between consecutive frames were performed by matching detected blisters to existing tracks using a cost-minimization approach. Track positions were first predicted using the Kalman filter, and a cost matrix was computed between predicted and detected objects based on: distance between centroids, changes in area and aspect ratio, orientation difference, and spatial overlap (after dilation). Assignments were determined using the Hungarian algorithm with a maximum cost threshold. To ensure physically meaningful matches, associations were accepted only if overlap with the previous object (after dilation) exceeded 20%.

Track management: Matched tracks were updated using new measurements and Kalman filter correction. Unmatched tracks were terminated after three consecutive missed frames, and new tracks were initialized for unmatched detections. In merging events, only one track was continued, while others were terminated. Splitting events were flagged and terminated, marking the end of a blister.

Post-processing filters: Tracks shorter than three consecutive frames were discarded. Tracks exhibiting abrupt area reductions greater than 40% in successive frames were truncated at the point of change. Final geometric measurements were converted from pixel units to physical units using calibration parameters.

Manual track curation: Tracked blisters were overlaid on the original MT fluorescence images and visually inspected. Results were manually corrected where necessary to ensure consistency with the underlying data.

Characteristic blister width analysis: Tracked blisters were analyzed over time, and for each blister, the maximum width observed across its lifetime was determined. The characteristic width w at each DNA_k was then defined as the mean of these maximum widths across all tracked blisters.

Characteristic wavelength analysis: For each blister, the nearest-neighbor centroid-to-centroid distance was measured across its lifetime. The steady-state characteristic wavelength, λ, defined as the mean of these distances computed from frames in which $\geq 85\%$ of the maximum number of blisters in a sample were detected, was calculated at each DNA_k.

Blister width analysis: For each DNA_k concentration, 20 blisters from a single sample were selected, and their widths were measured manually at a representative point along each blister. The mean width at each relevant DNA concentration was then calculated from these values. This methodology was used for the data Fig. 2c due to the lower resolution of the data set.

2.3 **Quantification of kinesin expression from GFP fluorescence:** To estimate kinesin production, GFP expression was compared with and without kinesin co-expression. A constant concentration of GFP coding plasmid ($0.4\,nM$, T7 promoter) was co-expressed with varying concentrations of kinesin coding plasmid ($0.1 - 9\,nM$, T7 promoter), enforcing competition for shared transcriptional and translational resources (T7 RNA polymerase, ribosomes, Amino acids, nucleic acids). Fluorescence was measured over time and converted to GFP-equivalent protein concentration using a calibration curve. Kinesin concentration, $[kinesin]$, at every time point was inferred from the reduction in GFP expression upon co-expression, $\Delta[GFP]$, reflecting resource diversion to kinesin synthesis. This GFP-equivalent signal was converted to kinesin concentration using a molecular weight-based scaling factor:

$$[kinesin] = \frac{\Delta[GFP]}{a};\ a = \frac{MW_{kinesin}}{MW_{GFP}}$$

Using $MW_{GFP} \sim 27\ kDa$ and $MW_{kinesin} \sim 55\ kDa$, we estimated $a \sim 2$. Based on three independent repeats, a plasmid concentration of 3 nM was found to correspond to the production of ~3 μM kinesin monomers after 6 hours of expression. This corresponds to ~1.5 μM dimers and ~750 nM tetrameric motor clusters (Fig. S3).

Conversion of fluorescence to concentration: To quantify kinesin expression in the CFE system, purified GFP fluorescence was used as a calibrated fluorescence unit for molar protein concentration. A calibration curve was generated using purified GFP at known concentrations (0-5 μM), imaged under known microscope settings as the expression experiment above (objective,

illumination intensity, binning, exposure time, and camera parameters). After background subtraction, fluorescence intensity was converted to molar concentration via linear regression. Each calibration point represents the mean of three independent repeats.

3. Model overview

We model three cell-free gene circuits that regulate kinesin motor production and translate motor concentrations into predicted MT flow speed. Each circuit is described by a system of ordinary differential equations (ODEs) governing mRNA and protein concentrations.

1. **Circuit 1 (constitutive kinesin expression):** Kinesin is expressed constitutively from a T7 promoter, with mRNA turnover and translation without protein degradation.
2. **Circuit 2 (kinesin with PRC1-mediated mechanical loading):** Kinesin (expressed under a T7 promoter) and the passive crosslinker PRC1 (expressed under a the p_{70} promoter) are expressed independently. Kinesin concentration determines the baseline active stress, while PRC1 modulates the resulting MT flow through an additive load-dependent stall factor that captures PRC1-induced mechanical friction.
3. **Circuit 3 (activator-repressor circuit with shared degradation capacity):** The activator protein A (a kinesin-σ^{28} fusion) is expressed constitutively and transcriptionally repressed by a repressor R (CI)[9]. Repressor expression is activated by A via Michaelis-Menten kinetics. Both A and R are degraded by a shared protease pool (ClpXP), modeled through an effective concentration-dependent lifetime $\tau_{XP}(A, R)$ that captures competition for finite degradation capacity.

All simulations are performed over 8 hours, with time in the ODEs expressed in minutes.

3.1 **Common transcription-translation assumptions:** All circuits are modeled using coarse-grained rate equations appropriate for CFE transcription-translation systems (**Table S2**). Transcription is assumed to scale linearly with DNA template concentration D, with promoters-specific effective transcription rates k_{TX}. All mRNA species undergo first-order decay characterized by a common lifetime τ_m. Translation is proportional to mRNA abundance, with an effective translation rate k_{TL}.

Protein degradation is treated in a circuit-dependent manner. In Circuits 1 and 2, proteins are assumed to be stable on experimental timescales, and no explicit protein degradation is included. In Circuit 3, protein turnover is mediated by a shared ClpXP protease pool, modeled explicitly through a concentration-dependent effective lifetime (see below).

3.2 **Modeling framework and biological context:** The gene circuits are modeled in an *E. coli* transcription-translation CFE system using effective mass-action and Michaelis-Menten kinetics for transcriptional regulation, translation, and degradation. This approach follows established coarse-grained ODE models for gene networks in lysates, in which molecular complexity is

compressed into experimentally measurable rate constants and regulatory thresholds[9,10]. All rates and concentrations used for the model are summarized in **Tables S2,S3**.

In CFE transcription-translation, untagged proteins are effectively stable, whereas SsrA-tagged proteins are selectively degraded by the ClpXP protease. mRNA lifetimes in this system are typically on the order of 10-20 minutes. Transcription from the σ^{70} promoter (p_{70}) is driven by endogenous *E. coli* RNA polymerase and facilitated by the abundant σ^{70} present in the CFE reaction mixture. Transcription from T7 promoters is driven by supplemented T7 RNA polymerase.

3.3 **Numerical integration and mechanical readout:** All circuits are simulated over an 8-hour duration using numerical integration (ode15s). The resulting protein concentration dynamics are mapped to predicted microtubule flow speeds using a nonlinear Hill-type transfer function. Where applicable, this baseline motor-driven flow is further modulated by a phenomenological factor that captures PRC1-dependent mechanical loading.

Circuit 1: Constitutive expression of kinesin under the T7 promotor (Fig. S14). The equations governing constitutive kinesin expression are:

$$\frac{dm_k}{dt} = k_{TX}^{T7} D_k - \frac{m_k}{\tau_m}, \tag{1}$$

$$\frac{dK}{dt} = k_{TL} m_k - \gamma_{k_{12}} K, \tag{2}$$

where m_k denotes the kinesin mRNA concentration, k_{TX}^{T7} is the effective transcription rate driven by T7 RNA polymerase, and D_K is the experimentally controlled concentration of the T7-kinesin DNA template, and τ_m is the mRNA lifetime in the CFE transcription-translation reaction. The kinesin protein concentration is denoted by K, with translation occurring at a rate K_{TL}. The term $\gamma_{K_{12}}$ represents a first-order kinesin loss or disassembly rate, which is set to zero in the present model, consistent with the stability of untagged kinesin in the extract.

Circuit 2: Constitutive kinesin expression with PRC1-mediated mechanical loading. Circuit 2 extends Circuit 1 by introducing constitutive expression of the passive crosslinker PRC1 alongside kinesin (Fig. S15). Kinesin is expressed from a T7 promoter, while PRC1 is expressed independently from a σ70 dependent p_{70} promoter. The transcriptional dynamics of the two genes are uncoupled, and their interaction enters only through the mechanical readout of microtubule flow.

The circuit is described by the following equations:

$$\frac{dm_k}{dt} = k_{TX}^{T7} D_k - \frac{m_k}{\tau_m}\ , \tag{3}$$

$$\frac{dK}{dt} = k_{TL} m_k - \gamma_{k_{12}} K \,, \tag{4}$$

$$\frac{dm_p}{dt} = k_{TX}^{70} D_P - \frac{m_p}{\tau_m} \,, \tag{5}$$

$$\frac{dP}{dt} = k_{TL} m_p - \gamma_p p \,. \tag{6}$$

Here, m_K and m_P denote the mRNA concentrations of kinesin and PRC1, respectively, and $K$and P denote the corresponding protein concentrations. The parameters K_{TX}^{T7} and K_{TX}^{70} represent the effective transcription rates driven by T7 RNA polymerase and endogenous *E. coli* RNA polymerase with σ^{70}, respectively. D_K and D_P are the experimentally controlled concentrations of the T7-kinesin and p_{70}-PRC1 DNA templates. All mRNAs decay with a common lifetime τ_m, and translation proceeds at a rate K_{TL}.

The parameters γ_{k12} and γ_p represent first-order protein loss rates for kinesin and PRC1, respectively. In the present model, both are set to zero, consistent with the stability of untagged proteins in the CFE.

Circuit 3: Activator-repressor gene circuit: kinesin-σ^{28} feedback with CI repression + ClpXP degradation. Circuit 3 implements an activator-repressor feedback architecture in which a kinesin-σ^{28} fusion protein acts as an activator that both drives mechanical output and regulates its own expression through a CI repressor (Fig. S15). The circuit dynamics are described by

$$\frac{dm_A}{dt} = k_{TX}^{70} D_A \cdot Rep(R) - \frac{m_A}{\tau_m} \,, \tag{7}$$

$$\frac{dA}{dt} = k_{TL} m_A - \frac{A}{\tau_{XP}(A,R)} \,, \tag{8}$$

$$\frac{dm_R}{dt} = k_{TX}^{28} D_R \cdot Act(A) - \frac{m_R}{\tau_m} \,, \tag{9}$$

$$\frac{dR}{dt} = k_{TL} m_R - \frac{R}{\tau_{XP}(A,R)} \,. \tag{10}$$

Here, m_A and m_R denote the mRNA concentrations of the activator and repressor, respectively, and A and R are the corresponding protein concentrations. The activator A is a kinesin-σ^{28} fusion protein expressed from a T7 promoter and transcriptionally repressed by the CI repressor R. The repressor R is expressed from a σ^{28}-dependent promoter p_{28} and is activated by A.

Regulatory interactions are modeled as

$$Rep(R) = \frac{1}{1+\left(\frac{R}{K_I}\right)^4} \,,$$

$$Act(A) = \frac{A}{K_A + A},$$

where K_I is the effective repression threshold for CI binding and K_A is the activation threshold for σ^{28}-driven CI expression. The Hill coefficient is consistent with the known cooperativity of CI repression.

Protein degradation of both A and R is mediated by a shared ClpXP protease pool and is modeled through a concentration-dependent effective lifetime, which captures competition for finite protease capacity, and is described by the following equation:

$$\tau_{XP}(A, R) = \frac{K_{deg} + A + R}{V_{max}}.$$

Here, V_{max} is the total zero-order degradation capacity of ClpXP (typically 20-100 nM/min for SsrA-tagged substrates), and K_{deg} is the Michaelis constant for ClpXP-mediated degradation. This formulation is algebraically equivalent to competitive Michaelis-Menten degradation of A and R by a shared enzyme pool.

4. **Flow concentration model:** To relate gene-circuit output to active microtubule transport, we model the mean MT flow speed $v(t)$ as a deterministic function of the instantaneous concentration of force-generating motors and passive mechanical regulators.

In all circuits, kinesin activity is assumed to generate extensile stresses that drive MT motion. The baseline flow speed is taken to increase monotonically with kinesin concentration and to saturate at high motor density:

$$v_0(k) = v_{max}\left(\frac{K^{n_v}}{K_{\frac{1}{2}}^{n_v} + K^{n_v}}\right),$$

where K is the concentration of active kinesin motors (nM), v_{max} is the maximal attainable MT speed, $K_{1/2}$ is the motor concentration at half-maximal speed, and n_v controls the sharpness of the transition and is ampirically reported. This Hill-type form captures cooperative force generation at low motor density and saturation due to filament crowding, motor interference, or force balance at high density (Fig. S16).

3.5 **Addition of PRC1 protein:** When passive crosslinkers (PRC1) are present, kinesin-generated stresses are mechanically filtered by crosslink-mediated coupling and friction. The effective flow speed is written as

$$v(K, P) = v_0(K) \cdot S(P)$$

with a PRC1-dependent mechanical multiplier

$$S(P) = \frac{1}{1 + \left(\frac{P}{P_s}\right)^h}.$$

This function satisfies:

- $S(P = 0) = 1$, indicating that no PRC1 implies no mechanical slowing;
- $0 < S(P) < 1$ for all P, ensuring that the slowing factor remains bounded;
- $S(P) \to 0$ as $P \to \infty$, corresponding to load-induced stalling.

The parameter P_S sets the PRC1 concentration at which flow is reduced by half, and h controls the sharpness of the transition.

Tables

Construct Name	Promoter	Gene / Feature	Source / Construction Method
p_{T7}-KIF3A	T7	Chimeric kinesin KIF3A expresses mouse kinesin-2 KIF3A head and neck linker, dimerized through kinesin-1 neck-coil to 406	KIF3A406 was a gift from William Hancock (Addgene plasmid # 129768).
p_{70}-deGFP	σ^{70}	deGFP reporter	[11]
p_{28}-CI-SsrA	σ^{28}	CI repressor of σ^{70} promoter	[9]
p_{70}-σ^{28}	σ^{70}	Transcription factor σ^{28} of *E.coli*	[9]
p_{T7}-deGFP	T7	deGFP reporter	This study. Cloned p_{T7} promotor via QuikChange mutagenesis on #40019.
p_{T7}-KIF3A-deGFP	T7	Kinesin-deGFP fusion	This study. Gibson assembly of KIF3A from #129768 fused to deGFP from #40019.
p_{70}-KIF3A-σ^{28}	σ_{70}	Kinesin-σ^{28} transcription factor fusion	This study. p_{T7} replaced with P_{70} promoter via QuikChange mutagenesis on (#129768), followed by Gibson assembly of the σ^{28} transcription factor from p_{70}-σ^{28} [12].
p_{70}-KIF3A-σ^{28}-SsrA	σ_{70}	Kinesin-σ^{28} fusion tagged with SsrA	This study. C-terminal SsrA addition via PCR on p_{70}-KIF3A-σ^{28}.
P_{70}-PRC1	σ_{70}	PRC1	Constructed by PCR. PRC1 gene taken from [8].

Table S1: Plasmids and DNA constructs used in this study. List of all plasmids used, including promoter type, encoded gene or functional element, and source or cloning method. Constructs were either obtained from Addgene or generated in this study using QuikChange mutagenesis, Gibson assembly, or PCR-based modifications.

Parameter	Unit	Definition	Value	Reference
τ_m	min	mRNA lifetime	12 min	[13]
k_{TX}^{T7}	$min^{-1} \cdot nM^{-1}$	Transcription from T7 dependent promoter	0.15	[5,13]
k_{TX}^{28}	$min^{-1} \cdot nM^{-1}$	Transcription from σ^{28} dependent promoter	0.1	[9]

k_{TX}^{70}	$min^{-1} \cdot nM^{-1}$	Transcription from σ^{70} dependent promoter	0.15	[13]
k_{TL}	min^{-1}	Protein production from mRNA (all circuits)	1	
D_k, D_P, D_A, D_R	nM	DNA concentrations	10-changing	
$\gamma_{K1,2}$	min^{-1}	Linear loss for kinesin protein K (circuits 1-2)	0	[13]
γ_P	min^{-1}	Linear loss for PRC1 protein P (circuit 2)	0	
K_A	nM	MM activation for R transcription: $\frac{A}{K_A+A}$, reduced because of the binding to the kinesin	50	[5,13]
K_I	nM	Hill repression scale in $Rep(R)$	2	
n		Cooperativity of repression of the CI protein	4	[9,10,13]
V_{max}	$\frac{nM}{min}$	Range for shared degradation pool construction	10-60 set at 20 to get oscillations	[5]
K_{deg}	nM	Shared-substrate competition scale in τ_{XP}	200	[5]

Table S2 : Model parameters used in the gene circuit simulations. List of parameter definitions, values, and literature references used in the protein-level gene circuit model. Parameter names correspond to those implemented in the simulation code.

parameter	Value	Units	
v_{max}	0.5	$\mu m/s$	Maximum MT flow speed
$K_{1/2}$	300	nM	Kinesin level for half-maximal flow
n_v	2	–	Cooperativity of kinesin-driven flow
P_f	600	nM	PRC1 level giving half-stall $S = 1/2$
h	3	–	Sharpness of stall transition

Table S3: Parameter values used for numerical simulations in figures. List of parameter values used to generate the simulation results shown in Figs. S10-S13. Parameter names correspond to those defined in Table S2.

References

1. Castoldi, M. & Popov, A. V. Purification of brain tubulin through two cycles of polymerization–depolymerization in a high-molarity buffer. *Protein Expr. Purif.* 32, 83–88 (2003).

2. Tayar, A. M., Lemma, L. M. & Dogic, Z. Assembling Microtubule-Based Active Matter. *Methods in Molecular Biology* 2430, 151–183 (2022).

3. Sanchez, T., Chen, D. T. N., Decamp, S. J., Heymann, M. & Dogic, Z. Spontaneous motion in hierarchically assembled active matter. *Nature* 491, 431–434 (2012).

4. Henkin, G., DeCamp, S. J., Chen, D. T. N., Sanchez, T. & Dogic, Z. Tunable dynamics of microtubule-based active isotropic gels. *Philos. Trans. A Math. Phys. Eng. Sci.* 372, (2014).

5. Garamella, J., Marshall, R., Rustad, M. & Noireaux, V. The All E. coli TX-TL Toolbox 2.0: A Platform for Cell-Free Synthetic Biology. *ACS Synth. Biol.* 5, 344–355 (2016).

6. Karzbrun, E., Tayar, A. M., Noireaux, V. & Bar-Ziv, R. H. Programmable on-chip DNA compartments as artificial cells. *Science (1979).* 345, 829–832 (2014).

7. Batista, A. C. *et al.* Differentially Optimized Cell-Free Buffer Enables Robust Expression from Unprotected Linear DNA in Exonuclease-Deficient Extracts. *ACS Synth. Biol.* 11, 732–746 (2022).

8. Subramanian, R. *et al.* INSIGHTS INTO ANTI-PARALLEL MICROTUBULE CROSSLINKING BY PRC1, A CONSERVED NON-MOTOR MICROTUBULE BINDING PROTEIN. *Cell* 142, 433 (2010).

9. Tayar, A. M., Karzbrun, E., Noireaux, V. & Bar-Ziv, R. H. Synchrony and pattern formation of coupled genetic oscillators on a chip of artificial cells. *Proc. Natl. Acad. Sci. U. S. A.* 114, 11609–11614 (2017).

10. Karzbrun, E., Tayar, A. M., Noireaux, V. & Bar-Ziv, R. H. Programmable on-chip DNA compartments as artificial cells. *Science (1979).* 345, 829–832 (2014).

11. Shin, J. & Noireaux, V. Efficient cell-free expression with the endogenous E. Coli RNA polymerase and sigma factor 70. *Journal of Biological Engineering 2010 4:1* 4, 8- (2010).

12. Tayar, A. M., Karzbrun, E., Noireaux, V. & Bar-Ziv, R. H. Synchrony and pattern formation of coupled genetic oscillators on a chip of artificial cells. *Proc. Natl. Acad. Sci. U. S. A.* 114, 11609–11614 (2017).

13. Karzbrun, E., Shin, J., Bar-Ziv, R. H. & Noireaux, V. Coarse-Grained Dynamics of Protein Synthesis in a Cell-Free System. *Phys. Rev. Lett.* 106, 048104 (2011).

Figures

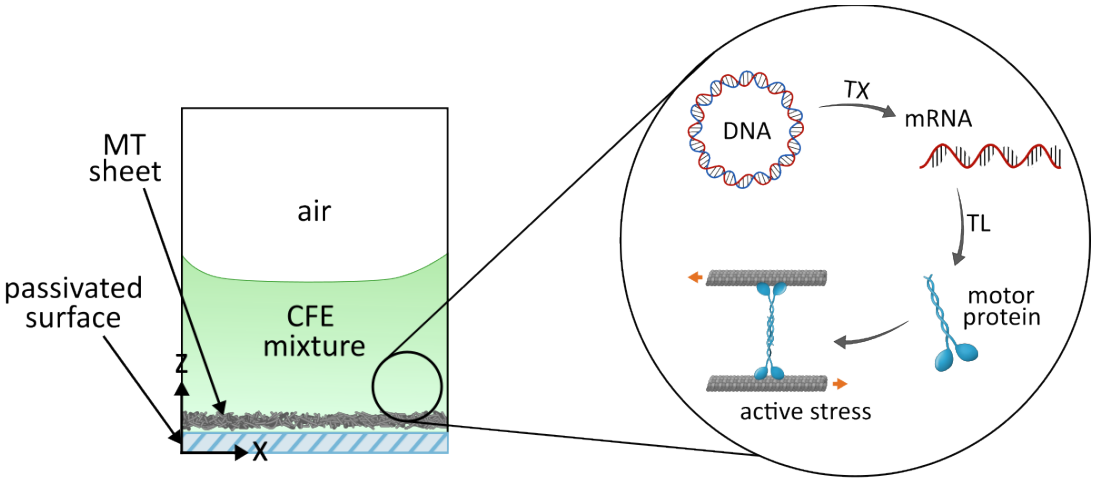

Figure S1: Experimental platform for cell-free microtubule-associated protein synthesis. Schematic of the CFE-MT system geometry. The CFE mixture contains DNA templates encoding MT-associated proteins, including motor proteins. The well bottom surface is passivated to reduce nonspecific protein adsorption. A dense, quasi-two-dimensional MT layer forms at the base of the well, establishing an active interface where newly synthesized proteins can directly interact with the MT network.

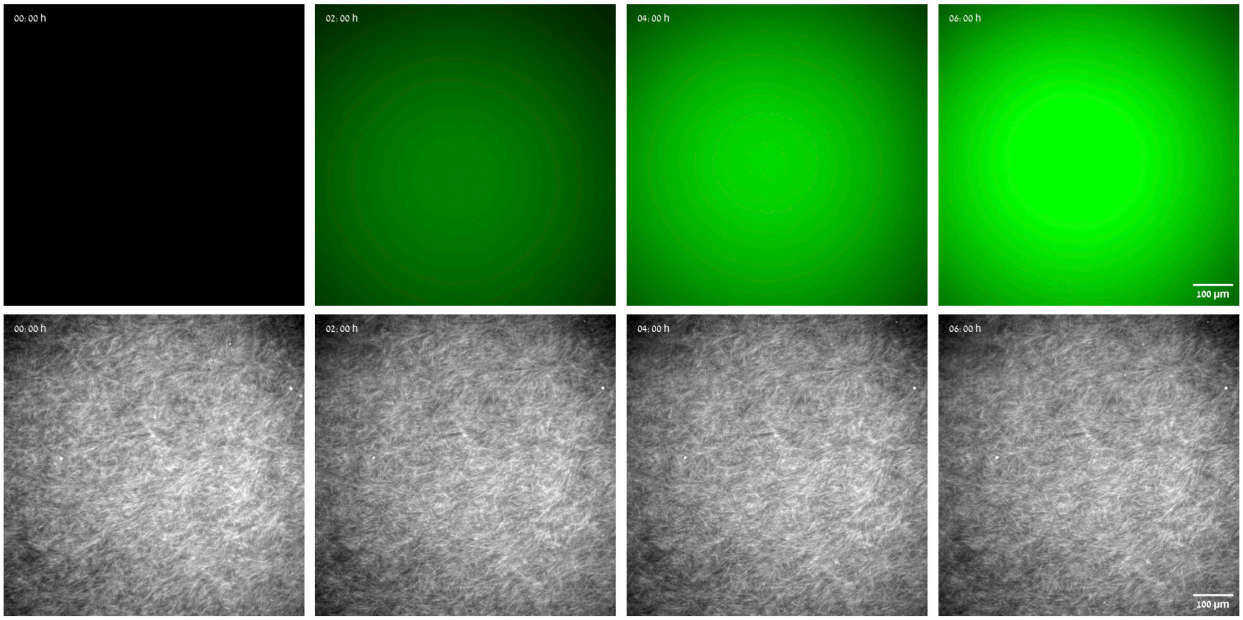

Figure S2: GFP protein expression in the presence of a microtubule sheet does not generate flow. Time-lapse images of GFP expression (green) driven by the T7 promoter in the presence of a microtubule sheet (grayscale) sedimented at the bottom of the well. No kinesin was expressed in this experiment. Scale bar: $100\ \mu m$.

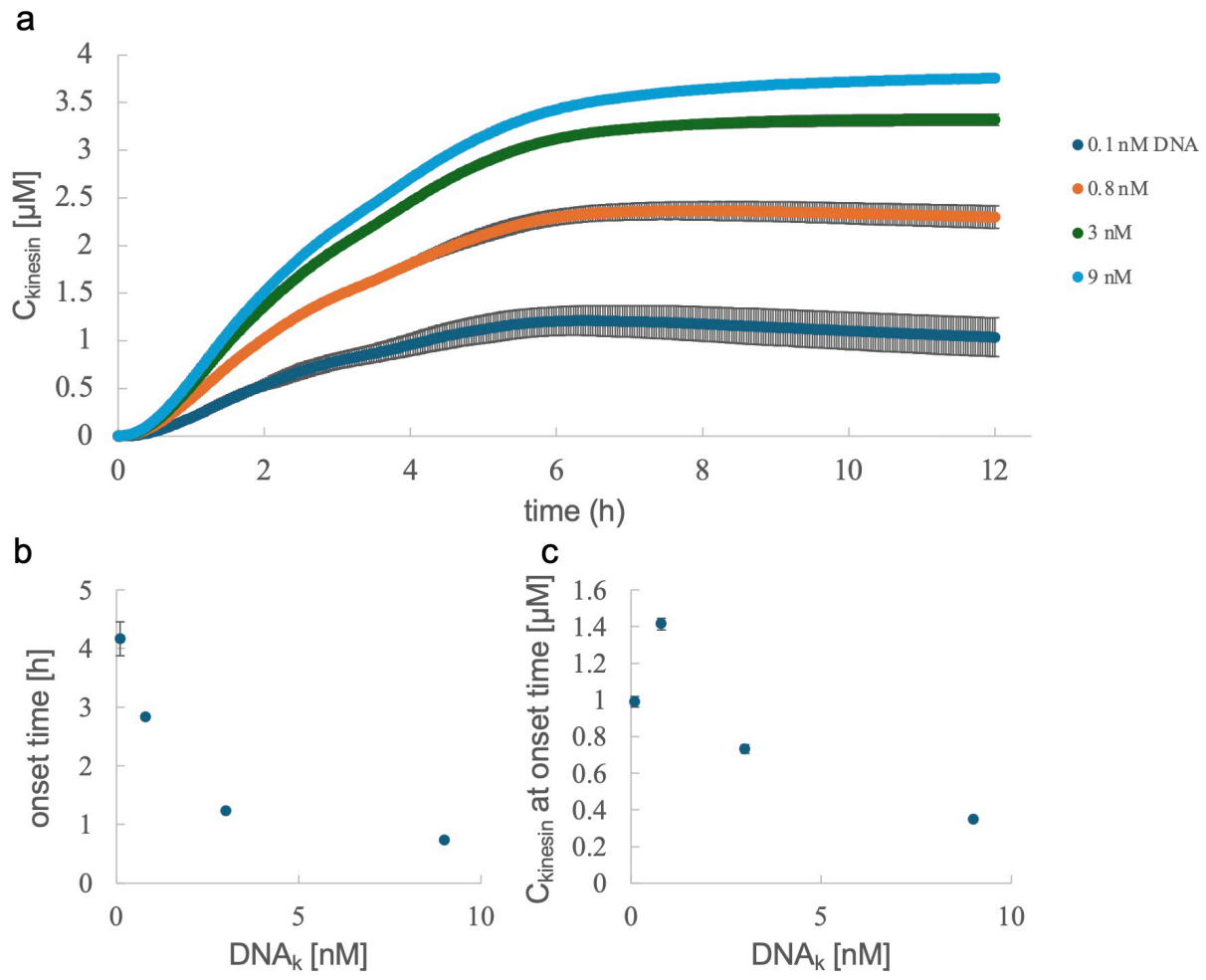

Figure S3: Kinetics of kinesin production as a function of DNA concentration in a cell-free system. (a) Kinesin concentration estimated from the reduction in GFP expression in the presence versus absence of kinesin co-expression, with both constructs driven by a T7 promoter. Measurements were performed at four kinesin DNA concentrations ($0.1 - 9\,nM$) with a constant GFP plasmid concentration of $0.4\,nM$. Fluorescence was converted to absolute kinesin concentration using a purified GFP calibration curve and corrected for differences in molecular weight between GFP and kinesin (SI). (b) Onset time of active flow in the microtubule sheet as a function of kinesin DNA concentration. (c) Kinesin concentration at the onset of flow estimated from (a), plotted as a function of kinesin DNA concentration. Error bars represent standard deviation from three independent repeats.

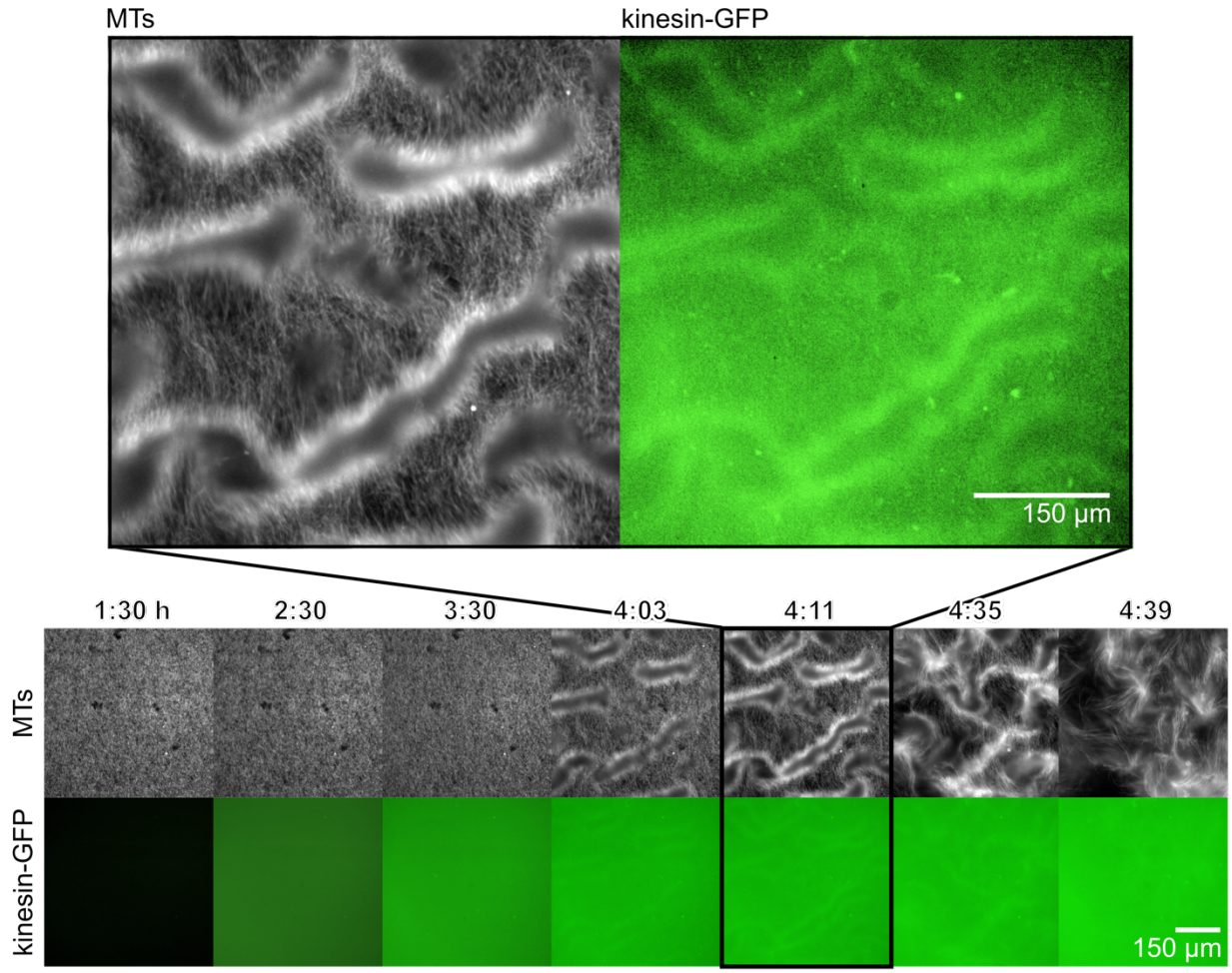

Figure S4: Time-lapse imaging of kinesin-driven active microtubule (MT) flows. Expression of a kinesin-GFP fusion (green) is shown alongside corresponding MT sheet images (grayscale), illustrating the emergence and evolution of active flows over time. The kinesin-GFP fusion was expressed under a T7 promoter, constituted ~13% of the total kinesin population, and was co-expressed with unlabeled kinesin to promote tetramer formation and motor activity. Experiment was performed at 0.7 nM kinesin DNA and 0.1 nM kinesin-GFP DNA. The initially homogeneous MT network evolved into aligned bundles and subsequently developed dynamic, chaotic flow patterns characteristic of MT-based active matter. Scale bar: 150 μm.

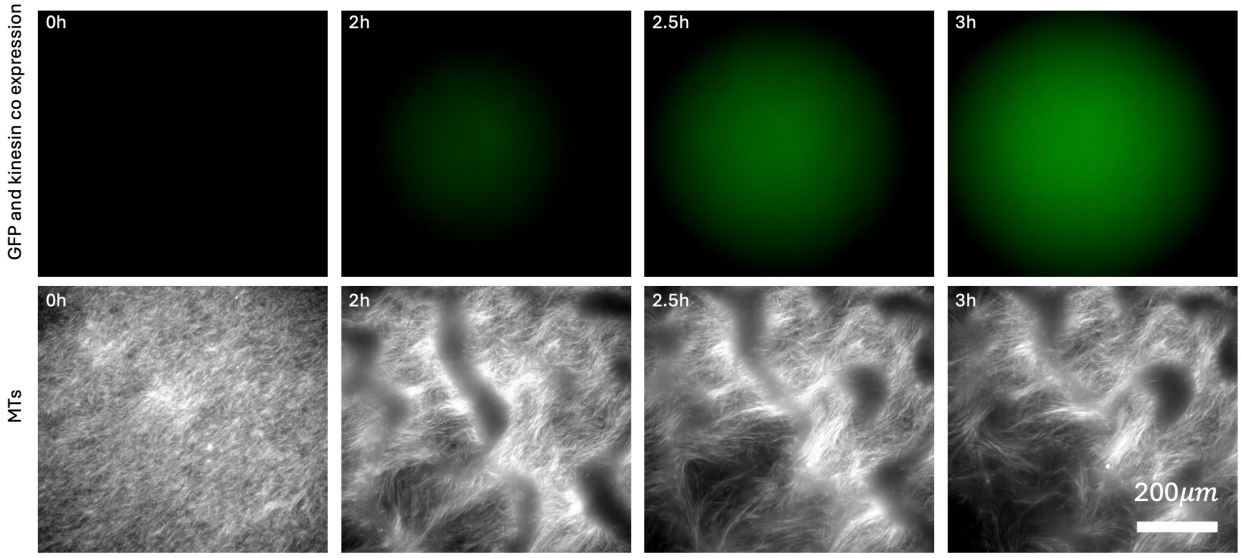

Figure S5: Time-lapse imaging of GFP co-expression with kinesin (no fusion). Expression of GFP (green) is shown alongside corresponding MT sheet images (grayscale), illustrating the emergence and evolution of active flows over time without detectable localization of GFP to the MT sheet. Both kinesin and GFP were expressed under a T7 promoter. Experiment was performed at 0.5 nM GFP DNA and 2.1 nM kinesin DNA. Scale bar: 200 μm.

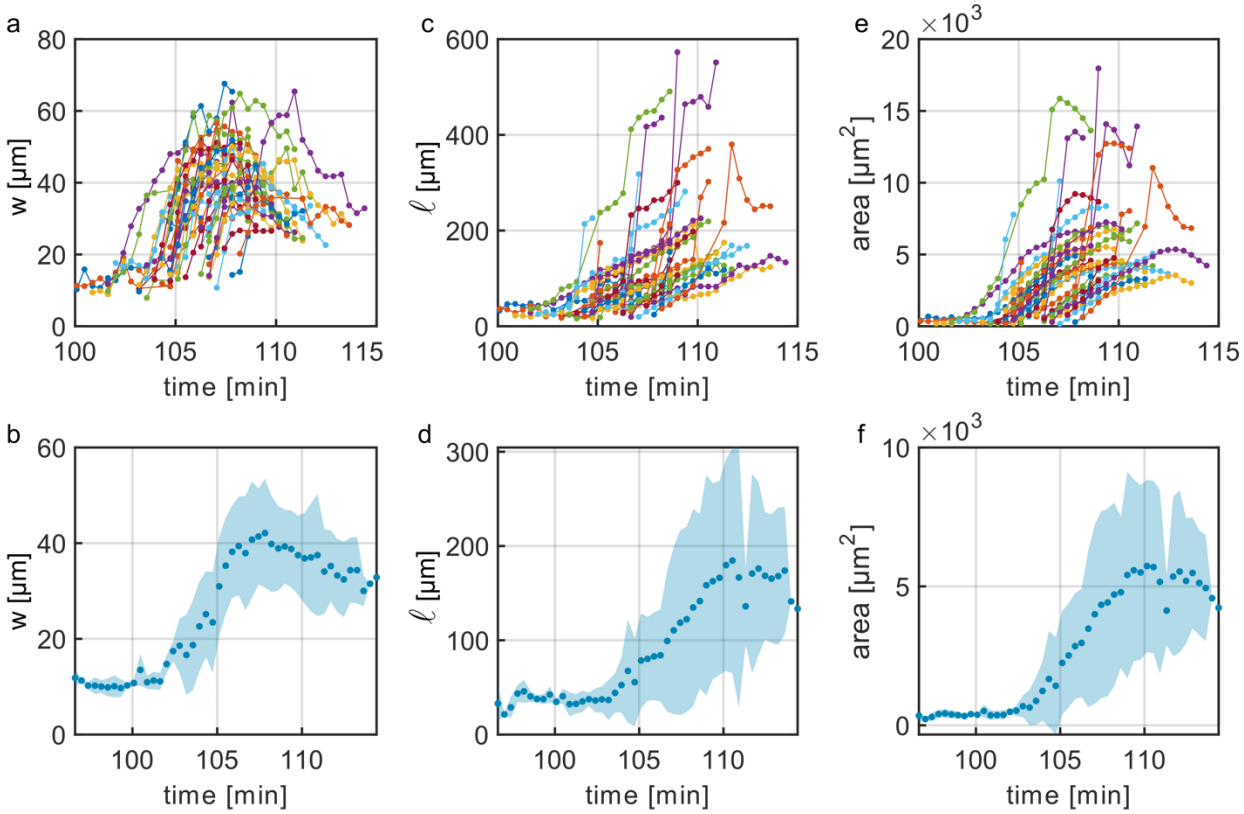

Figure S6: Dynamics of bending instability growth. (a) Individual blister widths as a function of time, with each color representing a single blister event. (b) Mean blister width (from data in (a)) as a function of time, showing a well-defined peak followed by relaxation; the shaded area denotes the standard deviation. (c) Individual blister lengths as a function of time. (d) Mean blister length as a function of time, with standard deviation (shaded region), showing sustained growth until blisters close. Data are averaged over all traces in (c). (e) Individual blister areas as a function of time. (f) Mean blister area as a function of time, with standard deviation (shaded region), showing an initial increase followed by saturation at a maximum size prior to blister closing. Data are averaged over all traces in (e).

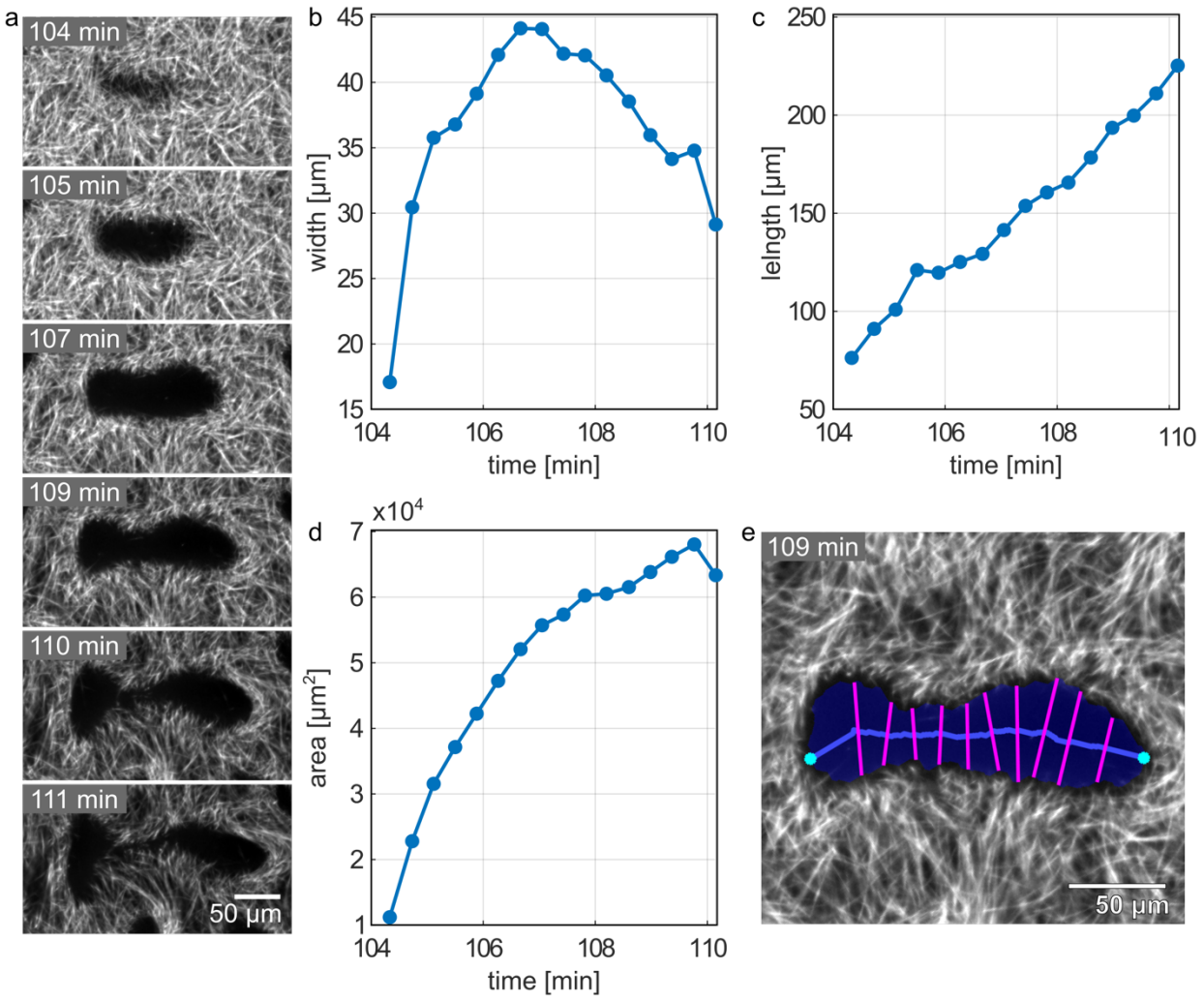

Figure S7: Planar dynamics of a single blister. (a) Time-lapse imaging showing the growth of a localized buckling instability in a microtubule network, evolving from an initially small deformation into an elongated blister-like structure, driven by constitutive expression of kinesin under a T7 promoter, and culminating in blister closure. Quantitative analysis tracks the temporal evolution of the blister (b) width, (c) length, and (d) area. (e) The segmented contour of the blister interface geometry at 109 min, with local normals (magenta) used to characterize the spatial structure of the deformation. Scale bar: 50 μm.

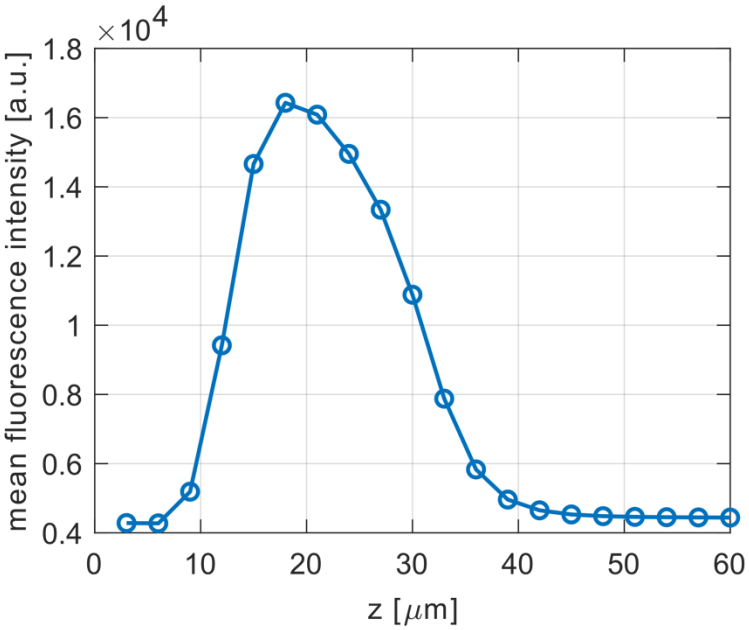

Figure S8: Estimation of MT sheet thickness. Confocal side-view fluorescence intensity profile of a microtubule sheet, used to estimate a sheet thickness of $h \sim 10\ \mu m$.

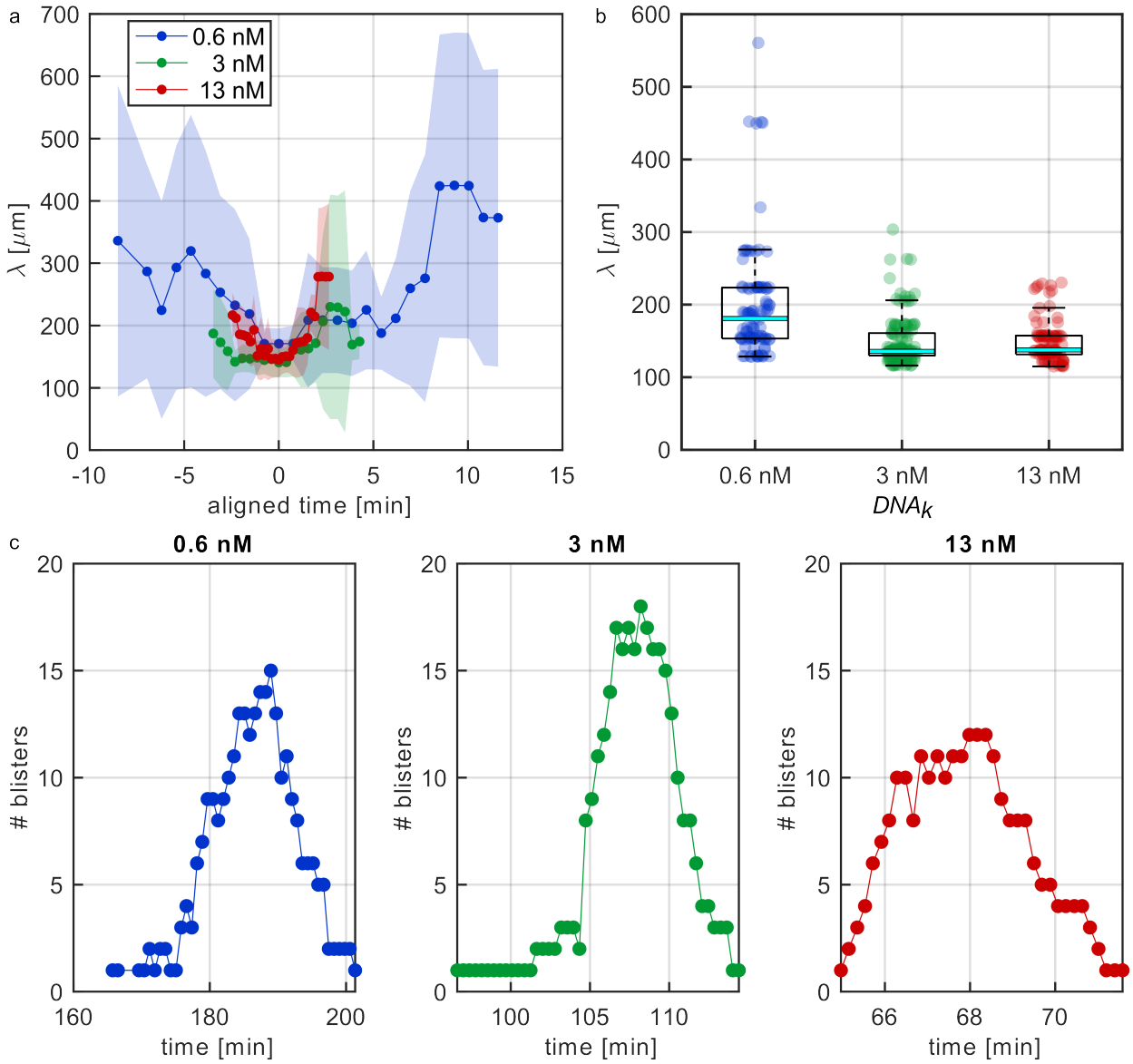

Figure S9: Characteristic wavelength of the buckling instability for different kinesin DNA concentrations. (a) Nearest-neighbor centroid-to-centroid blister distance, λ, aligned to the time of minimum steady-state wavelength, for three kinesin DNA concentrations (0.6, 3, and 13 nM) as a function of time. Shaded regions indicate standard deviation over $10-18$ blisters. (b) Distribution of steady state λ values, defined from frames where $\geq 85\%$ of the maximum number of blisters in a sample were detected, for each kinesin DNA concentration. Box plots show the median (cyan) and interquartile range (box). The median lambda values are 181, 136, and 138 μm, for 0.6 μM, 0.3 μM, and 13 μM, respectively. (c) Temporal evolution of the number of detected blisters for each kinesin DNA concentration. The imaging field of view was adjusted for each concentration to yield a comparable number of blisters for analysis.

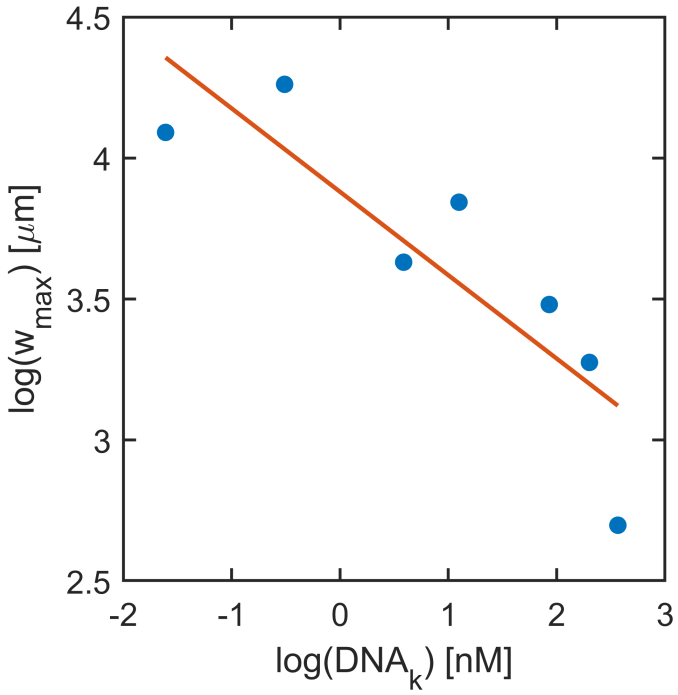

Figure S10: Scaling of bending instability width with DNA concentration. Log-log plot of the characteristic blister width, w, as a function of DNA concentration, c_{DNA_k}. Data points represent the mean of 20 blister widths from a single sample at each condition. The solid line shows a linear fit in log-log space, yielding corresponding to a scaling $w \propto C_{DNA_k}^{-0.29}$. This weak dependence indicates a sublinear relationship between kinesin DNA concentration and the selected instability length scale.

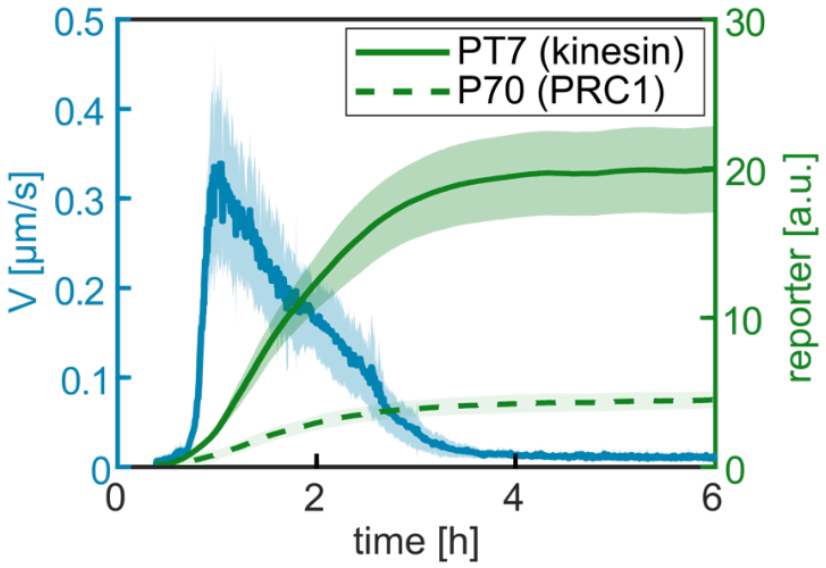

Figure S11: Mean velocity as a function of time during co-expression of kinesin and PRC1, complementary with data shown in Fig. 3c. The blue curve represents the mean velocity magnitude profile. Green curves show protein expression levels measured via GFP reporters: the solid line corresponds to GFP under T7 promoter (reporting kinesin production), and the dashed line corresponds to GFP under the P_{70} promoter (reporting PRC1 expression). Experiments were performed separately for each construct with three replicates each. shaded regions indicate standard error across replicates.

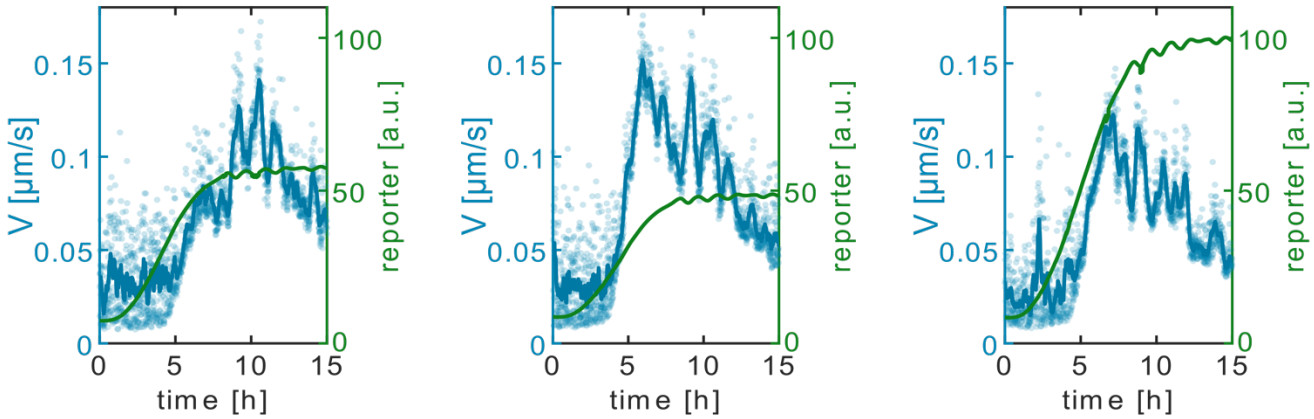

Figure S12: Oscillations in kinesin gene circuit activity with reporter expression. Three independent repeats showing oscillatory dynamics of the kinesin gene circuit, plotted as flow velocity (blue) and reporter expression (green) over time. Each panel corresponds to a single experiment. The circuit consists of kinesin fused to the σ^{28} activator, which drives expression of its own repressor, CI, forming a negative feedback loop. Both regulatory proteins carry SsrA degradation tags and are degraded by the endogenous ClpXP protease present at basal levels in the lysate. A co-expressed P70-GFP-SsrA reporter is used to track circuit activity. Oscillations in flow velocity correlate with reporter expression, although the presence of the reporter impacts circuit dynamics due to competition for the shared ClpXP degradation machinery. Consequently, full phase-space mapping was performed in the absence of the reporter.

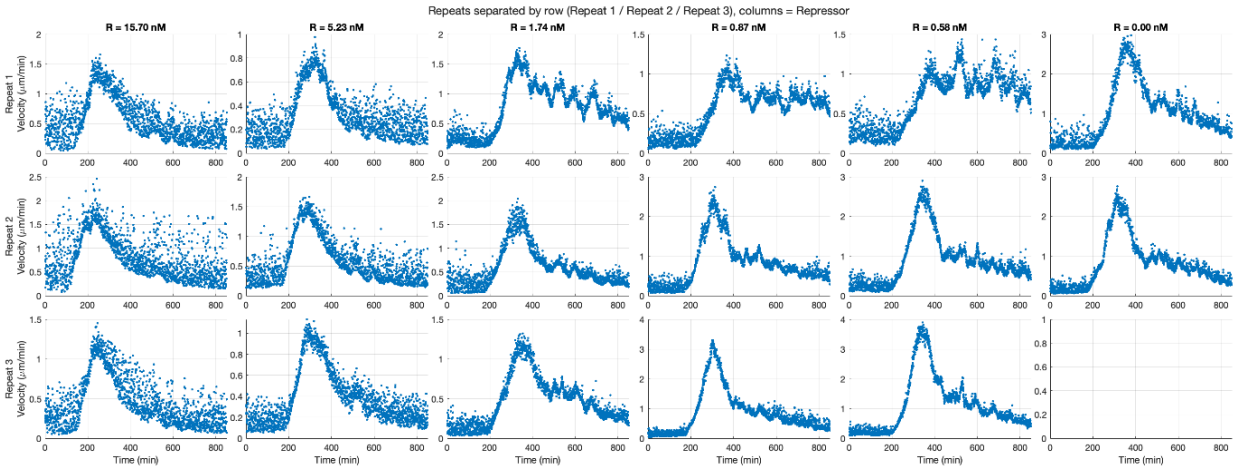

Figure S13: Velocity magnitude as a function of time for the activator-repressor gene circuit (data shown in Fig. 3e). Rows correspond to increasing concentrations of repressor DNA (R), while columns represent independent experimental repeats (Repeats 1-3). Activator-kinesin fusion gene is kept constant at a concentration of $20\,nM$. Data is shown for individual experiments without averaging to preserve the temporal dynamics. Variability between repeats arises from fluctuations in the ClpXP degradation machinery within the lysate.

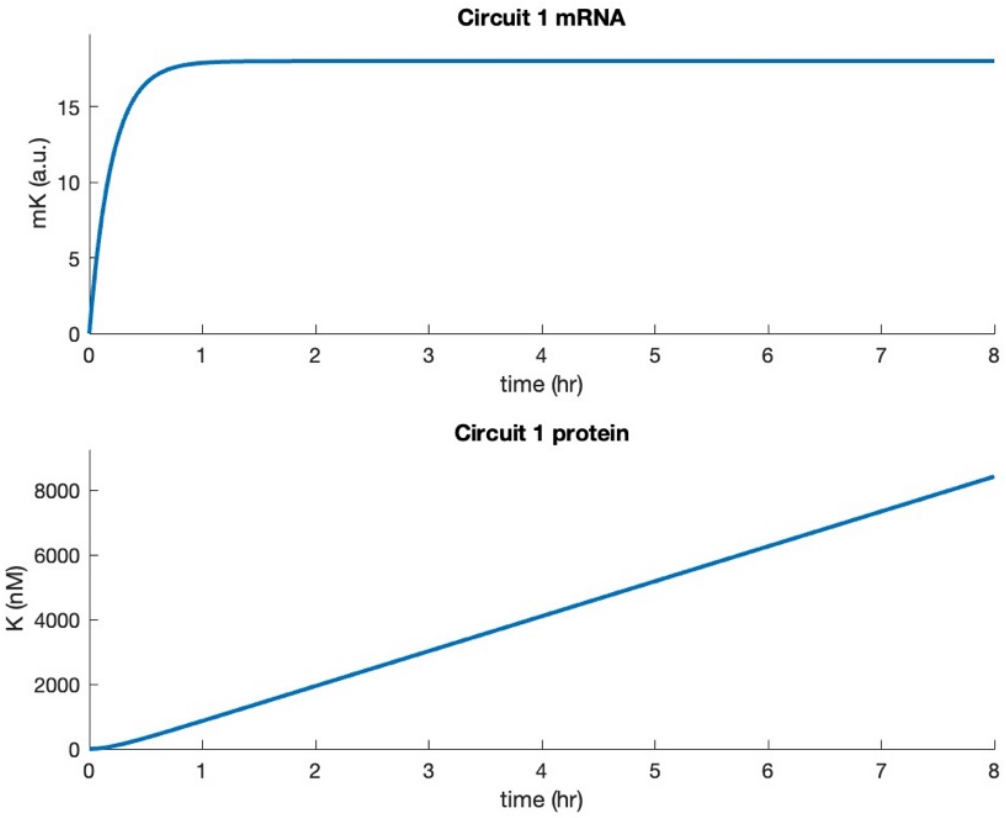

Figure S14: Simulated dynamics of the gene circuit shown in Fig. 3a, (Circuit 1 in the SI), illustrating kinesin mRNA and kinesin protein concentrations as functions of time for a DNA template concentration of $10\ nM$.

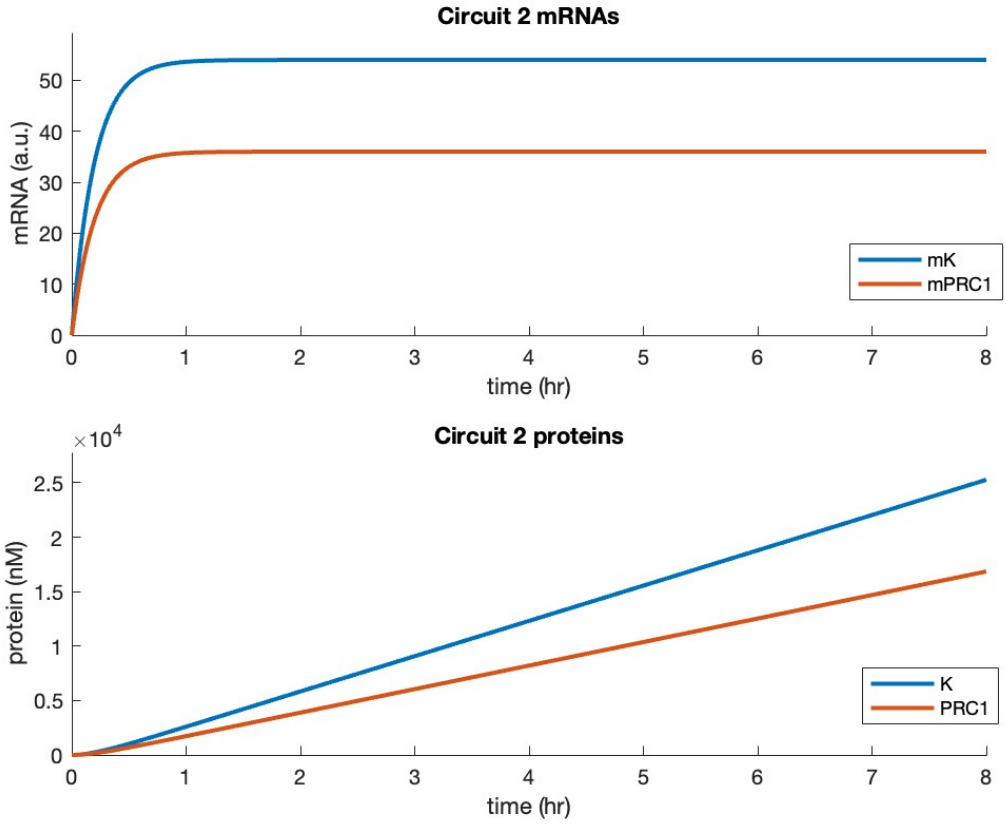

Figure S15: Simulated dynamics of the gene circuit in Fig. 3d (Circuit 2 in the SI) showing mRNA and protein concentrations during co-expression of kinesin (T7 promoter) and PRC1 (P_{70} promoter) for 30 nM kinesin DNA and 20 nM PRC1 DNA.

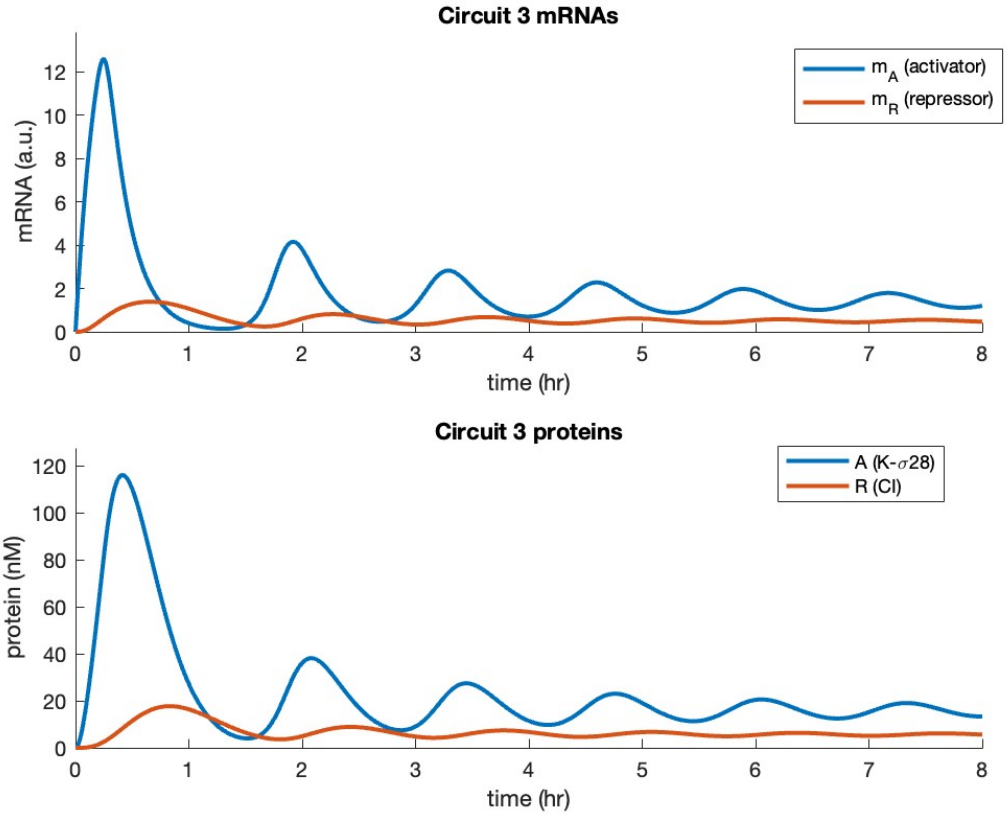

Figure S16: Simulated dynamics of the gene circuit in Fig. 3e (Circuit 3 in the SI), showing mRNA and protein concentrations of the kinesin-σ_{28} activator and CI repressor as functions of time for 15 nM activator DNA and 3 nM repressor DNA, with a ClpXP degradation capacity $V_{max} = 20\ nM/min$.

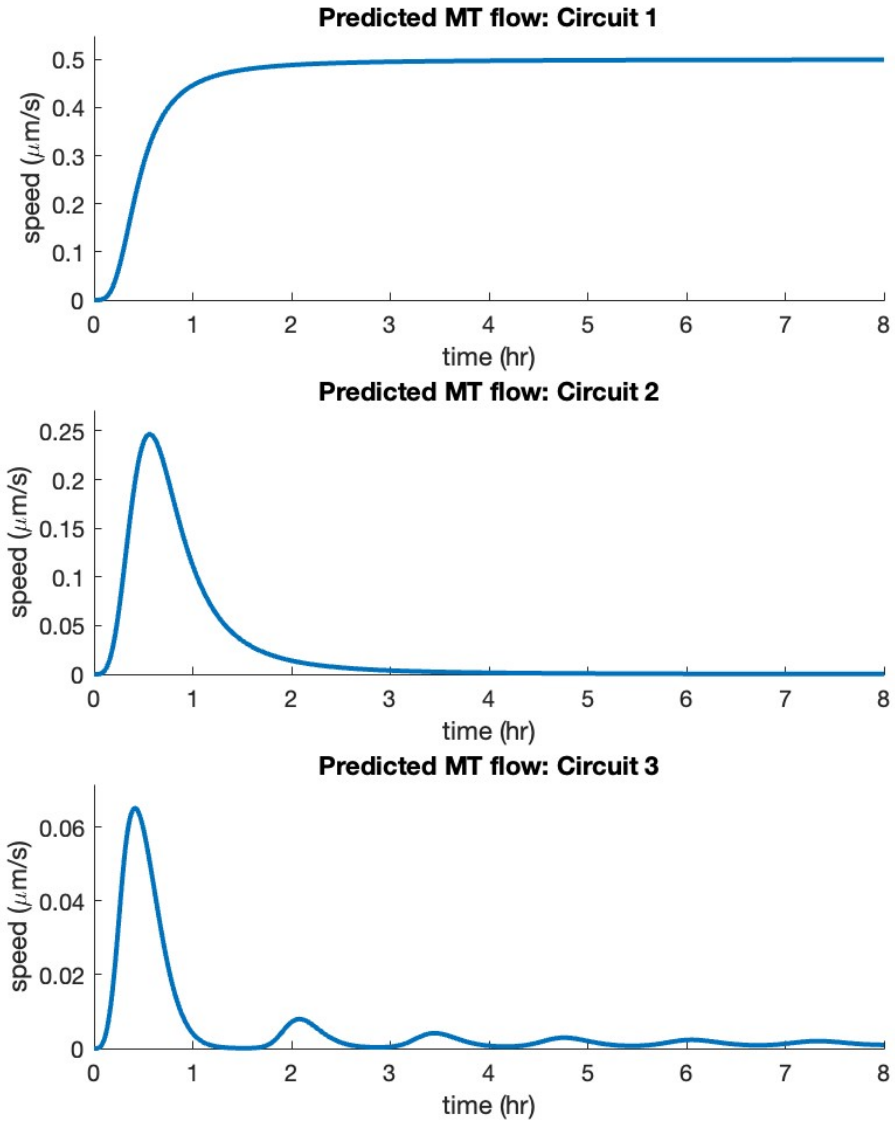

Figure S17: Predicted microtubule flow speeds computed from simulated protein concentrations shown in Figs. S10-S12, using the empirical flow-concentration model.

Video Captions

Video 1: 3D reconstruction of confocal time-lapse data showing constitutive kinesin expression from a T7 promoter. DNA concentration: $0.6\ nM$.

Video 2: Time-lapse of kinesin expressed from a T7 promoter in a 3D-printed well patterned with $10\ \mu m$ surface protrusions. DNA concentration: $3\ nM$.